Journal of Computer-Aided Molecular Design, 11 (1997) 317–332.

J-CAMD 405

Modelling of the binding site of the human m_1 muscarinic receptor: Experimental validation and refinement

Hélène Bourdon[a,*], Susanne Trumpp-Kallmeyer[b,*], Herman Schreuder[b], Jan Hoflack[b], Marcel Hibert[b] and Camille-Georges Wermuth[a,**]

[a]*Laboratoire de Pharmacochimie Moleculaire, Centre de Neurochimie du CNRS, 5 rue Blaise Pascal, F-67084 Strasbourg, France*
[b]*Synthélabo Biomoléculaire, BP 447 R/9, 16 rue d'Ankara, F-67080 Strasbourg, France*

Received 25 July 1996
Accepted 4 April 1997

Keywords: m_1 muscarinic receptor; Molecular modelling; Receptor–ligand interactions

Summary

Our model of the human m_1 muscarinic receptor has been refined on the basis of the recently published projection map of bovine rhodopsin. The refined model has a slightly different helix arrangement, which reveals the presence of an extra hydrophobic pocket located between helices 3, 4 and 5. The interaction of series of agonists and antagonists with the m_1 muscarinic receptor has been studied experimentally by site-directed mutagenesis. In order to account for the observed results, three-dimensional models of m_1 ligands docked in the target receptor are proposed. Qualitatively, the obtained models are in good agreement with the experimental observations. Agonists and partial agonists have a relatively small size. They can bind to the same region of the receptor using, however, different anchoring receptor residues. Antagonists are usually larger molecules, filling almost completely the same pocket as agonists. They can usually produce much stronger interactions with aromatic residues. Experimental data combined with molecular modelling studies highlight how subtle and diverse receptor–ligand interactions could be.

Introduction

Muscarinic receptors belong to the family of G-protein-coupled receptors (GPCRs) activated by acetylcholine [1]. Five distinct subtypes termed m_1–m_5 [2,3] have been identified. They are found in different areas of the brain and the periphery, and are likely to be involved in many different physiological processes. Agonists and antagonists able to discriminate receptor subtypes would represent very valuable pharmacological tools and potentially useful therapeutic agents. Particularly, m_1-selective agonists may be useful to enhance cognitive function in the treatment of Alzheimer's disease, whereas m_1-selective antagonists may behave as antiulcer drugs. The design of such compounds still remains a challenge. Molecular modelling combined with experimental structure–function relationship studies by site-directed mutagenesis might help to understand receptor–ligand recognition. We describe here three-dimensional (3D) models of agonists and antagonists binding to the human m_1 muscarinic receptor subtype. These models are qualitatively in good agreement with recent site-directed mutagenesis experiments on human m_1 muscarinic receptors (J.L. Paquet et al., personal communication).

Materials and Methods

Receptor modelling

Modelling was achieved with the commercially available SYBYL 6.04 and 6.1 software package [4]. The interactive modelling and display were performed on a Silicon Graphics 4D/280 computer.

The initial 3D model of the m_1 muscarinic receptor has been defined with the strategy and methods previously described [5]. Recently, a low-resolution map of bovine rhodopsin has been published [6] which confirms the

*H.B. and S.T.-K. contributed equally to this work.
**To whom correspondence should be addressed.

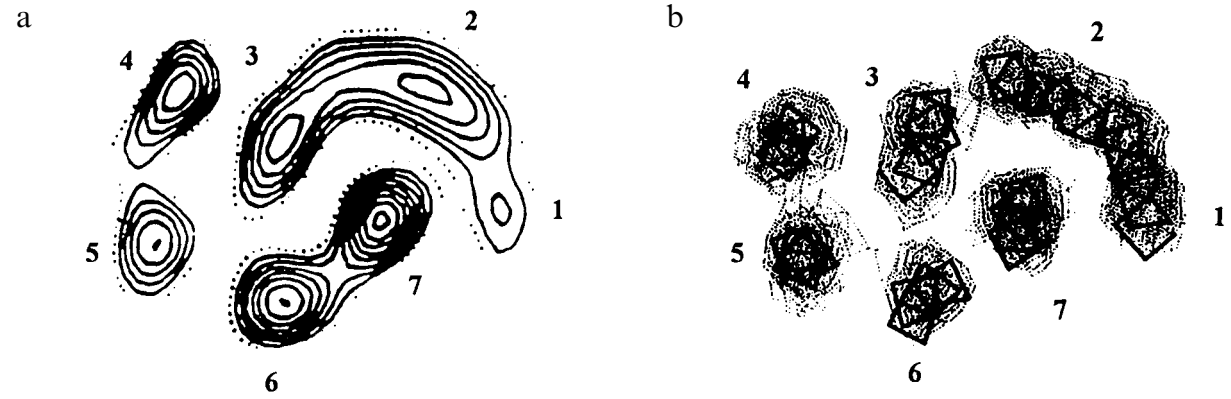

Fig. 1. (a) Electron density map of bovine rhodopsin. (Reprinted with permission from the concerned authors and from Nature [6]. Copyright 1993 Macmillan Magazines Limited.) (b) Theoretical electron density map of our refined 3D model of GPCRs, generated by X-PLOR. The two footprints are viewed from the extracellular surface.

seven-helix topology of GPCRs. Nevertheless, the relative positioning and tilt angles of the helices seem to be somewhat different from those found in bacteriorhodopsin (bR) [7,8]. Therefore, the existing human muscarinic m_1 receptor model was refined by repositioning by hand the seven transmembrane α-helices in order to obtain an optimal fit with the bovine rhodopsin footprint. For comparison with the published bovine rhodopsin footprint, a theoretical electron density map for the refined model was calculated with X-PLOR [9]. The complete model was placed in an artificial unit cell with axes of 100 Å and angles of 90°. Structure factors and phases were calculated between infinity and 8.0 Å and were then used to calculate the electron density map. The map was examined using FRODO [10]. The calculated electron density of the refined human m_1 receptor model shows a good match with the bovine rhodopsin projection map (Fig. 1). The relative tilt of the seven helices is now in good agreement with their 3D arrangement in the refined model proposed by Baldwin [8].

In the present study, an additional step in the modelling of the human m_1 muscarinic receptor was the building of the extra- and intracellular loops which connect the seven transmembrane-spanning α-helices of the receptor. The extracellular N-terminal end of the receptor, the three extracellular loops, and the first and second intracellular loops were built using the 'LOOP SEARCH' command available from the BIOPOLYMER module of SYBYL. We also built the disulfide bridge between Cys^{304} and Cys^{431} (the numbering of the residues of the human m_1 muscarinic receptor is depicted in bold in Fig. 2). Unlike the helical transmembrane domains that were fit with those of the rhodopsin footprint, the loops of the human m_1 receptor could not be fit with those of bR because of the difference in the sequence length. Therefore, they were built using a 'sequence homology' criterion and assembled in such a way that they had no bad steric interactions. The geometry of the complete structure was then optimized, first by rotating manually the dihedral angles of the side chains and subsequently by energy minimization for 2000 steps using the conjugate gradient minimizer and the Kollman 'All Atom' parameters of the AMBER force field installed in SYBYL [11]. In order to account to some extent for the membrane environment, a dielectric constant of 5 was chosen during the optimization procedure.

Small-molecule modelling

Three-dimensional models of the ligands used in the mutagenesis experiments (Fig. 3 and Table 1) were built from X-ray coordinates when they were available [12,13] or by using the standard fragments available in SYBYL (secondary and tertiary amines have been protonated). Regarding the m_1 receptor antagonists, the mutagenesis experiments were performed on three of the most potent ones: pirenzepine, NMS (*N*-methylscopolamine) and 4-DAMP (4-diphenylacetoxy-*N*-methylpyperidin methiodide). Some other antagonists could have been modelled, like the recently published FC 20-94 [14], but since the aim of our modelling study was to account for experimental data we restricted our computations to the tested compounds. In order to find a lowest energy conformation for each ligand, the conformational space of each compound was explored by a molecular dynamics simulation as follows. First, the charge distributions of the ligand structures were obtained with the semiempirical molecular orbital package MOPAC using the AM_1 approach [15] and Mulliken population analyses. Each charged structure was then minimized, and after charge recalculation of the optimized conformation the dynamic conformational search was performed at increasing temperatures and a constant pressure of 0 atm, with integration steps of 1 fs, using the Tripos force field. The structures were initialized at 10 K starting from a Boltzmann distribution followed by 1 ps of equilibration and 104 ps of simulation up to 1000 K. The conformations were

recorded every 1 ps and the charges were then recalculated before the minimization. In this way, the conformation with the lowest energy minimum was identified for each compound.

A more accurate method would consist in dynamic charge sets that follow the molecule as it changes conformation. In our computations however, by superimposing the different structures generated by our dynamic simulation method, we checked that, for each ligand, the conformational space was broadly covered, thus producing a representative sample of all the possible conformations.

Docking

In order to find common conformations of the studied compounds to help the docking procedure, we first redefined a pharmacophore for muscarinic agonists as described in the literature [16]. Using the 'active analogue approach' and the agonist oxadiazole **1** [17] as a reference, we superposed cationic heads and polar areas common to our set of muscarinic agonists (Fig. 3). We accepted a difference of 15 kcal/mol between the energy of the superposed conformer and the calculated lowest minimum-energy conformer of each compound, assuming that this additional energy can easily be compensated by the specific interactions established between the ligand and the receptor. Regarding the antagonists, no pharmacophore was identified since, in contrast to agonists, no muscarinic antagonist was rigid enough to be used as a template.

Conformers extracted from the superposition of the agonists and low-energy conformers of the antagonists were then separately and manually docked in the putative binding site, taking into account mutagenesis results (Table 1) and ligand structure–activity relationship studies. Thus, after establishing the ionic pair between the charged head group of the ligand and Asp^{311}, we systematically tried to establish one H-bond with Asn^{617} located on helix 6, for which the mutation to Ala was shown to decrease the affinity of agonists and antagonists (Table 1). H-bonds between Thr^{504} and agonists were not built due to the lack of effect seen by the mutation to an Ala. Side chains of the interacting residues were oriented in order to respect the putative active conformation of the ligands, as well as H-bond geometry (i.e. an angle of 120°–180° between the donor atom, the H-atom and the acceptor atom of the H-bond) and orientation of the lone pairs of electrons. The receptor–ligand complex was then minimized within a sphere of 10 Å around the ligand according to the optimization procedure described above. During this step, a dielectric constant of 1 was chosen, and the H-bonds were constrained by a distance range of 1.8–3 Å, and a force constant of 100. Our purpose was to account for mutagenesis data, especially the fact that mutation of Asn^{617} to Ala had a strong influence on the binding of agonists and antagonists. Therefore, this rather large value of 100 for the force constant was chosen to ensure the stability of the H-bond established between each ligand and Asn^{617}. No constraint was set on the ionic bond, to allow a more flexible positioning of the ligand during the optimization. Furthermore, no constraint was applied to the angular part of the H-bond, to check whether the correct geometry (i.e. an 'acceptor-H-donor' angle of between 120° and 180°) was maintained after minimization of the complex, thus indicating the plausibility of the H-bond.

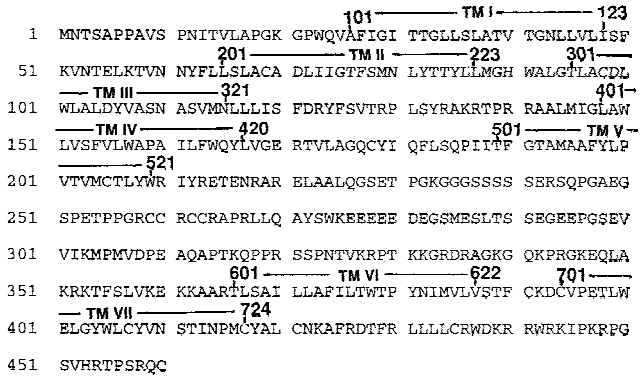

Fig. 2. Residue numbering in each of the seven transmembrane domains (TM) of the human m_1 muscarinic receptor: the first digit corresponds to the helical transmembrane domain and the next two digits indicate the position of the residue in the helix.

Results and Discussion

G-protein-coupled receptors play a critical role in many physiological processes. It is of prime importance to better understand their ligand structure–activity relationships and the receptor structure–function relationships in order to be able to modulate signal transduction phenomena.

Ideally, these relationships should be derived from high-resolution crystallographic structures of GPCR–ligand complexes to minimize speculations regarding the receptor–ligand interaction mode. However, access to such structural information still remains a challenge. Instead of waiting until such data become available, we have decided to generate novel hypotheses from theoretical structural models and to probe them experimentally with a combination of complementary techniques such as site-directed mutagenesis, chemical labelling, spectroscopy, mapping with ligands, etc.

Hence, we have proposed in 1991 [18] a general model for GPCRs based on the helix packing of bR and experimental data then available [19]. Most related experimental data published since are in good qualitative agreement with these first models.

The 3D structure of bR has recently been refined [20] to an R-factor of 28% at 3.5 Å resolution. In the refined coordinates, three of the six surface loops are clearly

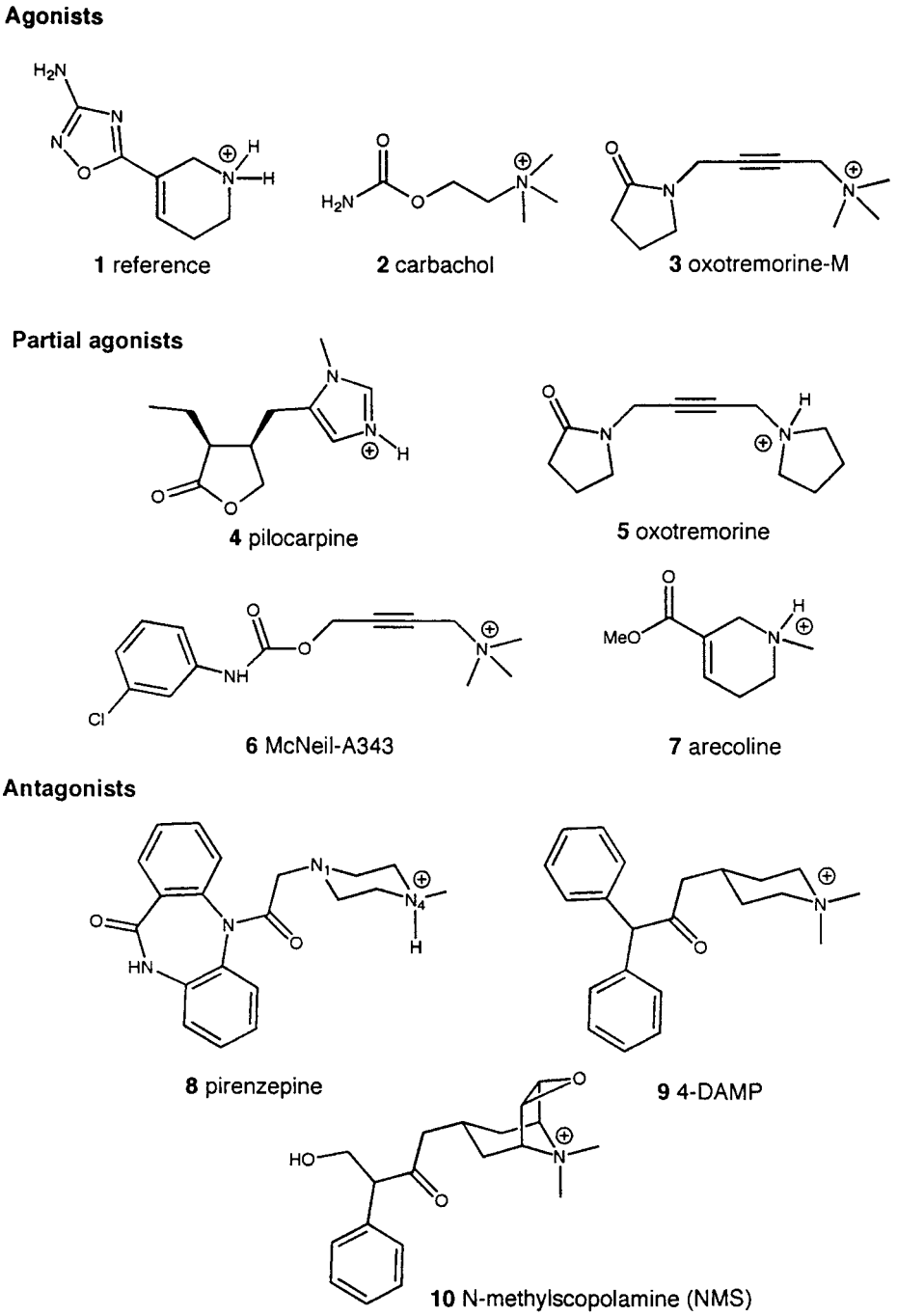

Fig. 3. Structure of the muscarinic ligands used for the site-directed mutagenesis experiments.

resolved. The relative positioning of the helices is the same as in the low-resolution structure, except for helix D (TM IV), which is in fact located 4 Å closer to the external side of the lipid bilayer.

Four years ago, the first experimental two-dimensional (2D) model of a GPCR, bovine rhodopsin, became available [6]. It confirmed the existence of seven transmembrane helices, but suggested that their packing is slightly different from bR [8]. Meanwhile, the putative binding site of human muscarinic m_1 receptor ligands proposed from the model has systematically been explored by site-directed mutagenesis (Table 1). We report here our refined model of GPCRs and how it accounts qualitatively well for new structural and biological experimental data.

Before entering into the presentation and discussion of the results, it might be useful to briefly review the potential and limitations of such an approach. Regarding the experimental data, site-directed mutagenesis results must be analyzed cautiously since the effect of a mutation can

be interpreted as the consequence of a direct interaction of the ligand with the mutated residue, or as an indirect effect via a conformational change of the receptor. Moreover, a fact that we cannot take into account is that the various single-point mutations might affect the equilibrium between the quiescent and activated states of the receptor [21]. Indeed, it was shown that active receptor states can be induced by mutations. It was also shown that an active receptor state activates G-protein without an agonist being bound and has a higher affinity for agonists but not for antagonists. Therefore, the decrease in the binding observed for antagonists could also be related to their lower affinity for the active receptor state, which can be induced by the mutation.

We have tried to minimize these problems by probing a whole region of the receptor and by focusing our interpretation to the differential effects of mutations on a series of ligands. The 3D models of GPCRs suffer from some obvious limitations. They have been derived by homology modelling from low-resolution experimental structures and cannot pretend to have a higher resolution than the original template (which is 3.5 Å parallel and 10 Å perpendicular to the membrane); the ligand affinity can be affected by many factors (coupling to G-protein; expression system and level; allosteric modulators; solvation; etc.) which cannot be taken into account; the dynamics of the receptor backbone cannot be simulated without empirical approximations; etc.

Taken together, these limitations indicate that these GPCR models have a qualitative value only and cannot quantitatively account for subtle differences in affinity and efficacy. Conscious of these issues but convinced of the usefulness of this approach, we report below our refined model of the muscarinic m_1 receptor–ligand complexes.

Muscarinic m_1 receptor model based on the bovine rhodopsin projection map

The model of the human muscarinic m_1 receptor based on the bovine rhodopsin projection map has a helix packing which is somewhat different from that observed for bR (Figs. 4a and b). In the bovine rhodopsin-derived models like in our human m_1 muscarinic receptor model (Fig. 4b), helices 4, 5, 6 and 7 are parallel to each other, with helices 1, 2 and 3 tilted by approximately 15°. Helices 3 and 5 lie closer together than in the bR-derived model, helix 4 being behind them. In contrast, in bR and hence in GPCR models based on it (Fig. 4a), helix 4 is roughly parallel to helices 2 and 3 rather than to helices 5, 6 and 7. In addition, helices 3 and 5 are further separated because helix 4 is positioned between them.

The different helix arrangement in bovine rhodopsin-derived models leads to a different size and shape of the binding pocket compared to bR. In GPCR models based on the bovine rhodopsin projection map, the binding cleft is wider and possesses an additional pocket defined by helices 3, 4 and 5. On the contrary, the binding cleft in the bR-derived GPCR models is narrower with one major pocket, defined by helices 2, 3, 4, 5, 6 and 7. The additional pocket is missing due to the different orientation of helices 3, 4 and 5.

In the refined human m_1 receptor model, helix 3 presents a slightly wider face to the inside of the pocket. In addition, only the last third of helix 1 (near the intracellular side) seems to participate in the transmembrane cleft, whereas the extracellular half has contact essentially with helices 2 and 7 and the lipid bilayer.

Despite these differences, the proposed binding residues of acetylcholine and other neurotransmitters [18] are the same in GPCR models based on bovine rhodopsin and on bR and are found at a similar depth in the extracellular

TABLE 1
K_I MUTANT/K_I WILD TYPE RATIO OF THE DIFFERENT TESTED AGONISTS AND ANTAGONISTS

Ligand	Trp^{307} →Phe	Trp^{307} →Ala	Tyr^{312} →Phe	Asn^{316} →Ala	Trp^{410} →Phe	Thr^{504} →Ala	Thr^{504} →Ala[a]	Trp^{613} →Phe	Trp^{613} →Ala	Asn^{617} →Ala	Ser^{718} →Ala	Thr^{719} →Ala
Agonists												
Carbachol	0.3[b]	0.9[b]	3.6[b]	8.3[b]	6[b]	2.5[b]	**31**	0.9[b]	0.2[b]	**>100**	1.5[b]	1.3[b]
Oxo-M	0.6[b]	**19.1**[b]	2.3[b]	**31.7**[b]	7.4[b]	2.7[b]		**0.1**[b]	0.8[b]	**>100**	2.1[b]	1[b]
Partial agonists												
Pilocarpine		0.6		3.2		0.8		4.8				
Oxotremorine		0.8		13.3		1		1.6				
McN-A343		0.7		0.7		0.3		**0.1**				
Arecoline		0.7		3.8		0.5		0.6				
Antagonists												
Pirenzepine	2.2[b]	**28.9**[b]	0.8[b]	6.4	**66.1**[b]	0.6		1.2[b]	**34.6**[b]	**>100**	1.5	0.9
4-DAMP	0.8[b]	**13.2**[b]	1.3[b]	10.4	**131.9**[b]	1.3	1	4.8[b]	**288.2**[b]	**>100**	1.1	0.5
NMS[c]	1.4	**9.7**	2.8	7.2	**96.7**	0.8	1	1.8	**115**	**105**	1.6	0.7

[a] Taken from Ref. 27, measured in the m_3 receptor subtype.
[b] Ratio IC_{50} mutant/IC_{50} wild type (K_I values could not be determined because the Hill coefficient was lower than 0.8).
[c] Ratio K_D mutant/K_D wild type.

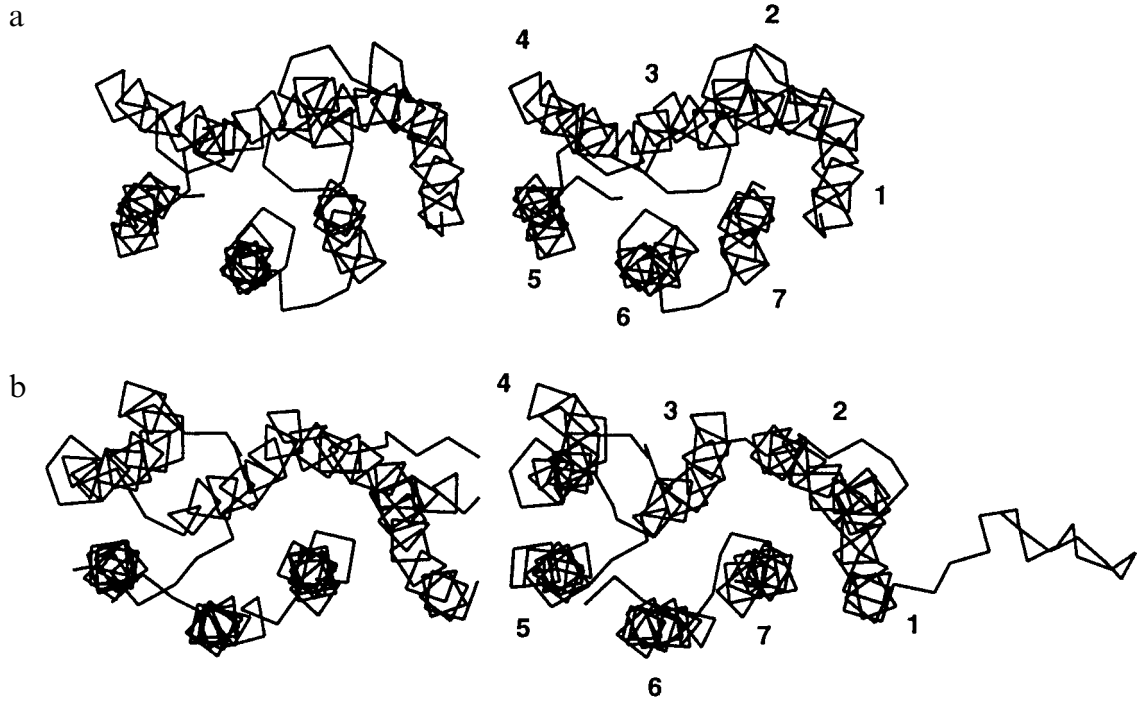

Fig. 4. Stereoviews, from the extracellular side, of (a) the refined 3D structure of bR (retrieved from the current release version of the PDB, available on the Internet: www.pdb.bnl.gov, id=2brd), and (b) our model of the human m_1 muscarinic receptor based on the bovine rhodopsin density map.

part of the transmembrane region. The amino acids conserved across all GPCRs are found essentially located in the cytoplasmic half of the receptor.

Like all cationic neurotransmitter receptors, the human m_1 receptor contains a highly conserved Asp residue on helix 3: Asp^{311} (see the alignment of GPCRs in Ref. 5) [22]. In the model, the ammonium-aspartate ion pair is surrounded by a series of conserved aromatic residues on helices 3, 4, 5, 6 and 7. The top of the binding cleft is formed by Trp^{307} located one helix turn above Asp^{311}, and Tyr^{432} located in the second extracellular loop after Cys^{431}, whereas Trp^{410}, Trp^{613} and Phe^{509} form the bottom of the cleft. The sides of this hydrophobic cluster are composed of residues Tyr^{616}, Trp^{707}, Tyr^{711}, Trp^{712} and Tyr^{312}. All these aromatic residues can form π-cation interactions with the positive head of the ligand, thus stabilizing the ionic pair and slowing down the ligand release. Furthermore, Tyr^{711}, Tyr^{715} and Tyr^{616} could also interact by their hydroxyl moiety with the charged nitrogen [5]. Particularly, the Tyr^{711}→Ala mutation has been shown to induce a decrease in affinity in the binding of acetylcholine, pirenzepine, NMS and 4-DAMP [23].

Besides this series of highly conserved aromatic residues, a number of conserved hydrogen bonding residues are also present in this pocket: Asn^{617}, Thr^{501}, Thr^{504}, Gln^{434} and Tyr^{432}. Among them, Gln^{434} and Tyr^{432} belong to the second extracellular loop. Indeed, the building of this loop shows that the disulfide bridge between Cys^{304} and Cys^{431} creates a connection between helix 3 and helices 4 and 5. This connection brings some additional rigidity to the system, especially around the binding site. In this way, some residues of the second extracellular loop, like Gln^{434} and Tyr^{432}, are in a favorable orientation towards the binding cleft. Although Gln^{434} is highly conserved in all muscarinic receptor subtypes, it was shown that mutation of this residue has no effect on the binding characteristics of the human m_2 receptor [24]. Tyr^{432} is present both in the human m_1 and m_2 receptor sequences and is conservatively replaced by a Phe residue in the human m_3 and m_4 receptor subtypes. Pointing closer to the binding site than Gln^{434}, Tyr^{432} could be one of the residues responsible for the ligand affinity. This hypothesis can be supported by the fact that there is mounting evidence that the second extracellular loop is also involved in the binding of agonists to small ligand GPCRs, such as adenosine receptors [25].

Site-directed mutagenesis experiments on muscarinic receptors

In the case of muscarinic receptors, site-directed mutagenesis experiments have shown that the residues responsible for the ligand anchoring are mainly the highly conserved Asp on helix 3, Asp^{311} (helix numbering), and polar residues located on helices 5 and 6. Indeed, the side chain of Asp^{311} was labelled by [^{3}H]propylbenzylcholine mustard [22], and its mutation to Asn, which abolished the charge property, elicited reduction of the affinity of both agonists and antagonists [26]. Regarding the second-

ary anchoring residues of muscarinic receptors, different studies have been performed essentially on the m_3 and m_2 subtypes.

In a study of the rat m_3 muscarinic receptor subtype, the hypothesis was made by Wess et al. [27] that the OH groups present in the side chains of the conserved hydrophilic residues may specifically interact via H-bonds with the electron-rich moieties common to all muscarinic ligands. In order to validate this hypothesis, the authors have created a series of single-point mutants in the rat m_3 receptor by converting serine and threonine residues to alanine, and tyrosine residues to phenylalanine. All these OH-group-deleting mutations led to a 10–40-fold decrease in agonist binding affinity compared to the wild-type receptor. The same mutations had only little or no effect on the binding affinity of the antagonists NMS and trihexylphenidyl, suggesting that muscarinic agonists and antagonists may bind to their receptor by different molecular mechanisms. Particularly, the two residues Thr^{504} and Tyr^{616}, which show the strongest decrease in agonist binding affinity after mutation, were proposed to interact via H-bonds with agonists, whereas a serine residue, Ser^{214}, seemed to be involved in an H-bond with antagonists. The corresponding mutant Ser^{214}→Ala bound both NMS and trihexylphenidyl with about 10-fold lower affinity than the wild-type receptor, while the binding of agonists was not affected by this mutation.

As for the rat m_3 receptor, in the case of the human m_2 receptor the threonine mutations on helix 5 (Thr^{501} and Thr^{504}) alter the binding of most agonists but not of antagonists [24].

A series of single-point mutations were performed on the human m_1 receptor by Matsui et al. [23] to probe the allosteric site where gallamine can bind and allosterically change the binding affinity of agonists and antagonists for the competitive site. From these studies, it was suggested that the allosteric site may be located close to and just extracellular to the antagonist binding site.

In order to probe the agonist competitive site compared to the antagonist binding site, various single-point mutations were performed on cloned human muscarinic m_1 receptors. Some amino acids thought to be involved in agonist binding were systematically converted into phenylalanine or alanine in the case of the conserved tryptophan and tyrosine, or only to alanine in the case of the hydrophilic asparagine, threonine and serine residues. The binding affinity of agonists, antagonists and partial agonists for the mutant receptors has been studied by competition with [^{3}H]NMS (Table 1).

From the mutation of Trp^{307} and Trp^{613}, it appeared that the binding of carbachol and arecoline is only slightly affected. In contrast, this was not the case for the agonist oxotremorine-M (oxo-M), whose affinity for the Trp^{307}→Ala mutant was decreased 19-fold. In addition, oxo-M and McNeil-A343 (McN-A343) bound to the Trp^{613}→Phe mutant receptor with higher affinity. This latter observation is in agreement with Wess's results [28], which showed that conversion of Trp^{613} to Phe in the rat m_3 receptor resulted in a mutant receptor with an acetylcholine binding affinity that was 20 times lower than that of the wild-type receptor. Thus, as was predicted by the former model of muscarinic receptors, Trp^{307} and Trp^{613} are most probably located in the agonist binding site. In addition, mutation of these residues to Ala strongly decreased the affinity of the three antagonists pirenzepine, 4-DAMP and NMS. Similarly, in a recent article [29], it was shown that mutation of Trp^{307} to Ala decreased the affinity of PZ by a factor of 155. It has also been reported by Matsui et al. [23] that acetylcholine, NMS, 4-DAMP and pirenzepine show a decreased affinity for the Trp^{307}→Ala mutant receptor. Thus, in agreement with the model, Trp^{307} and Trp^{613} may indeed interact with the cationic head of agonists and antagonists by forming cation-π complexes, as mentioned previously, or they may directly form hydrophobic interactions with the aromatic rings of antagonists. Mutation of Trp^{410} into Phe led to a moderate decrease in the binding of agonists. This is in agreement with a weak hydrophobic interaction between Trp^{410} and agonists, which is not changed much through the conservative mutation to a Phe residue. On the contrary, this mutation led to a strong decrease in the binding of pirenzepine, 4-DAMP and NMS, suggesting that the considered antagonists have much stronger interactions with Trp^{410} than agonists.

The most interesting result from this series of experiments is the finding that Asn^{617} plays a crucial role in the binding of antagonists. From the model, it was found that this residue, conserved in at least 32 GPCRs, including the muscarinic receptors [5], was ideally located to interact with the ester group of acetylcholine. In receptors activated by aromatic ligands such as dopaminergic, adrenergic, serotoninergic and histaminergic receptors, Asn^{617} is replaced by a highly conserved Phe. As predicted [18], site-directed mutagenesis studies demonstrated that this Phe is important for the binding of serotonin and adrenaline [30]. Asn^{617} was therefore proposed to be a crucial element in the binding of muscarinic ligands. Our site-directed mutagenesis experiments on the human muscarinic m_1 receptor show that the Asn^{617}→Ala mutant receptor displays a 100-fold decreased affinity for [^{3}H]NMS and that no reliable monophasic competitive displacement could be obtained with the considered agonists and antagonists. Interestingly, mutation of Thr^{504} to Ala in the m_1 receptor does not affect the affinity of agonists and antagonists. These results are different from those obtained by Wess on the rat m_3 receptor, where the Thr^{504}→Ala mutation induced a 40-fold decrease in the binding of agonists [27] whereas the Asn^{617}→Ala mutation had only a slight effect [31]. Although the binding affinities of (–)-QNB, 4-DAMP and trihexylphenidyl for the

Asn^{617}→Ala and Asn^{617}→Ser mutants were only moderately decreased (8–43-fold), the binding of subclasses of antagonists, including atropine-like agents and pirenzepine, was also drastically decreased (235–28 300-fold) by the Asn^{617}→Ala mutation in the m_3 receptor subtype [31]. In the human m_2 receptor subtype, it was shown that Asn^{617}→Ala is unable to bind [^{3}H]NMS and [^{3}H]QNB [22]. Thus, from these experimental results it can be concluded that, in the m_1, m_2 and m_3 receptor subtypes, the Asn^{617} residue on helix 6 clearly plays a role in the binding of antagonists. This residue is not involved in the binding of agonists in the m_3 receptor subtype and its contribution to the binding of agonists in the m_1 and m_2 receptor subtypes could not be proven, because of the low affinity of the tritiated ligand for the mutant receptor in the competitive experiments. However, as was already proposed in the case of the m_2 receptor subtype [5], in the 3D model of the m_1 receptor Asn^{617} is ideally located in the agonist environment. Due to this very favorable position in the binding site, and since Thr^{504} is not involved in the binding of agonists and antagonists, we have speculated that, in the case of the human m_1 receptor subtype, Asn^{617} plays a key role in the binding of both agonists and antagonists.

More generally, we can conclude that the considered agonists and antagonists bind to the same region of the human m_1, m_2 and m_3 receptors consisting of helices 2, 3, 4, 5, 6 and 7. However, different agonists may bind to different subregions and may form a different hydrogen bonding network, depending on their chemical structure and the receptor subtype.

It should be noted that the results of the different studies must be compared with extreme caution. It cannot be excluded that the different assay conditions used in the mutagenesis studies are responsible for the different results obtained for agonists. Moreover, different radiolabelled ligands have been used which might induce different conformational states of the receptors. Finally, the cell types and the incubation times were also different in the two experiments. Hence, it is not clear yet whether the differences observed are related to the receptor subtypes and to species differences only.

Muscarinic ligand docking: Agreement with experimental data

Taking into account our former model and the most recent results of Wess on the rat m_3 receptor, Nordvall and Hacksell [32] have proposed a model for the binding site of the human m_1 muscarinic receptor. Using a combination of homology-based modelling and indirect approaches, the authors proposed Asn^{617} and Thr^{504} for establishing H-bonds with the considered agonists. This model was attractive since it was able to accommodate agonists which were structurally different from those used to generate it and since it was able to differentially accommodate the two stereoisomers of muscarine. However, it does not fully account for the more recently disclosed experimental data on GPCRs in general [6], and on the m_1 receptor in particular (Table 1).

The most recent description of the interactions of the human m_1 receptor with a series of muscarinic ligands was made by Fanelli et al. [33]. In this article, a set of 34 agonists, partial agonists, weak partial agonists and antagonists were fitted into the binding cleft of the m_1 receptor model using Wess's mutagenesis results. Agonists and antagonists were docked in two different sites: the aromatic moiety of the tricyclic antagonists was docked near helices 2, 3 and 7 whereas agonists were fitted in the pocket built by helices 3, 4, 5 and 6. Partial agonists were fitted in between the agonist and antagonist binding domains, their orientation depending on the relative values of the NMS/oxo-M affinity ratio. Thus, in this model, agonist and antagonist binding sites are obviously different and share only Asp^{311} as a common anchoring point. The proposed QSAR model shows a good linear correlation between the intermolecular interaction descriptors (interaction energies) and the pharmacological action. However, this latest model is not consistent with more recent mutagenesis experiments (Table 1). Taking them into account, we can now put forward the hypothesis that the tested agonists and antagonists bind to the same region in the transmembrane cleft of the receptor. In the present work, our aim is to account qualitatively for these recent data by fitting the considered ligands in the active site of our refined 3D model of the human m_1 receptor.

As described, the pharmacophoric conformations of the nine compounds used in the site-directed mutagenesis experiments were fitted into the binding site according to the docking procedure described above. These conformations were not drastically changed after minimization of the ligand–receptor complex.

For all compounds, an ionic interaction of the cationic head with Asp^{311} could be established, together with one

TABLE 2
BINDING AFFINITIES OF THE MUSCARINIC LIGANDS FOR THE PARENT MUSCARINIC m_1 RECEPTOR

Muscarinic ligand	K_I (μM) [^{3}H]NMS
Agonists	
Carbachol	125
Arecoline	17.6
Oxo-M	9.9
McN-A343	8.69
Pilocarpine	5.1
Oxotremorine	0.967
Antagonists	
Pirenzepine	0.0116
4-DAMP	0.000896
NMS	0.000120[a]

[a] K_D (μM).

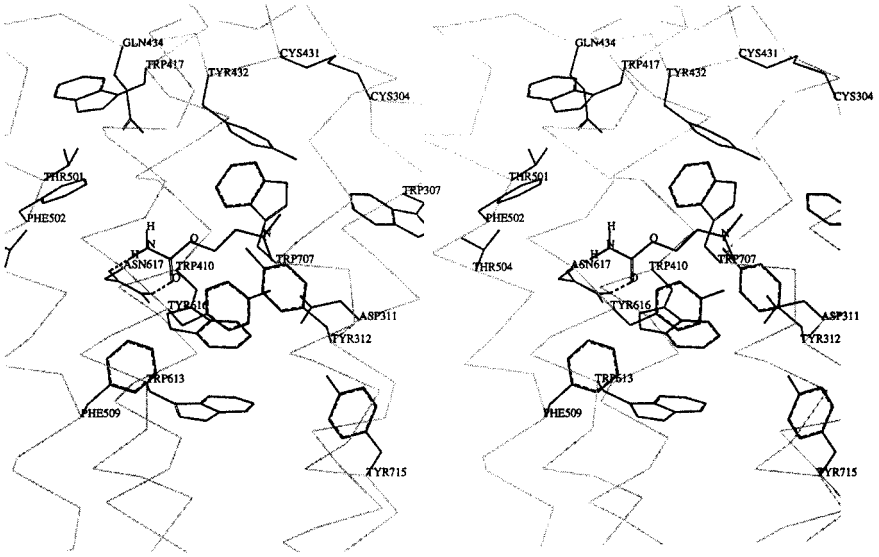

Fig. 5. Stereoplot of carbachol docked in the binding site of the m_1 muscarinic receptor. Only residues of the binding site and the main chain are displayed.

H-bond formed by a heteroatom of the molecule with the Asn^{617} residue. This finding is consistent with the electrostatic features proposed in the pharmacophore models [16,34]. It can be noted that in the minimized complexes, the geometry of the H-bonds was not changed very much, the angle between the donor, the hydrogen and the acceptor atoms still being in the range of 120°–180°. This indicates that, assuming the validity of our model of the human m_1 muscarinic receptor, our hypothesis of H-bonds between ligands and the Asn^{617} residue was a realistic one.

Regarding the ionic interaction, there are observable differences in the figures in the distance between the cationic head group of the ligand and Asp^{311}. This distance ranges from 3.9 to 5.1 Å. These differences have been allowed by the minimization procedure and depend on the presence of an additional H-bond with Asp^{311} (which shortens the ionic bond in the case of the protonated amines) and also on the structure of each ligand (which forces it to adopt specific interaction geometries and distances).

A second general remark that we can make from the observation of the different ligand–receptor complexes is the contrast between the variety of binding modes of the agonists and the more rigid and similar binding modes of the antagonists. This is actually supported by the binding affinities of the muscarinic ligands for the parent receptor, reported in Table 2. Indeed, there is an increase in the affinity from the agonists (K_I in the μM range) to the antagonists (K_I in the nM range), whereas the affinity of the partial agonists is between those of the agonists and those of the antagonists. These values suggest stronger interactions of the antagonists with the residues of the binding site.

Accordingly, in the model, the considered agonists, which are much smaller and more flexible than the antagonists, do not fill the whole agonist binding site of the receptor. Therefore, different agonists are able to interact with different subsites in the agonist binding pocket. As an example, carbachol can establish two H-bonds between its carboxamide function and the carboxamide function of the Asn^{617} side chain on helix 6 (Fig. 5). Not surprisingly, due to its small size, carbachol cannot establish strong interactions with the aromatic residues Trp^{307}, Tyr^{312}, Trp^{410} and Trp^{613}. Indeed, mutations of these residues only affect the binding affinity of carbachol by 0.2–6-fold (Table 1).

As a second example, oxo-M, which is larger than carbachol, is much more affected by the same mutations (Fig. 6). The Trp^{307}→Ala mutation was tested and effectively decreased the affinity 19-fold. In addition, the Trp^{613}→Phe mutation increased the affinity 10-fold and the Trp^{410}→Phe mutation decreased the affinity 7-fold. In the refined model, the carbonyl oxygen of oxo-M forms an H-bond with Asn^{617} and the quaternary ammonium group of oxo-M can form π-cation interactions with Trp^{307}. Trp^{410} can form additional π-cation and aromatic interactions with the molecule. The latter interactions are likely to be weaker, due to the larger interaction distance. The increase in affinity for the Trp^{613}→Phe mutation is rather difficult to understand: it might be due to a more indirect interaction.

Interestingly, the Trp^{307}→Ala mutation strongly decreased the affinity of oxo-M (19-fold), whereas it did not affect the binding of oxotremorine in spite of the ligand structural similarity. Once again, the 3D model of the receptor could qualitatively account for this difference in affinity. In the case of oxo-M, due to a larger interaction

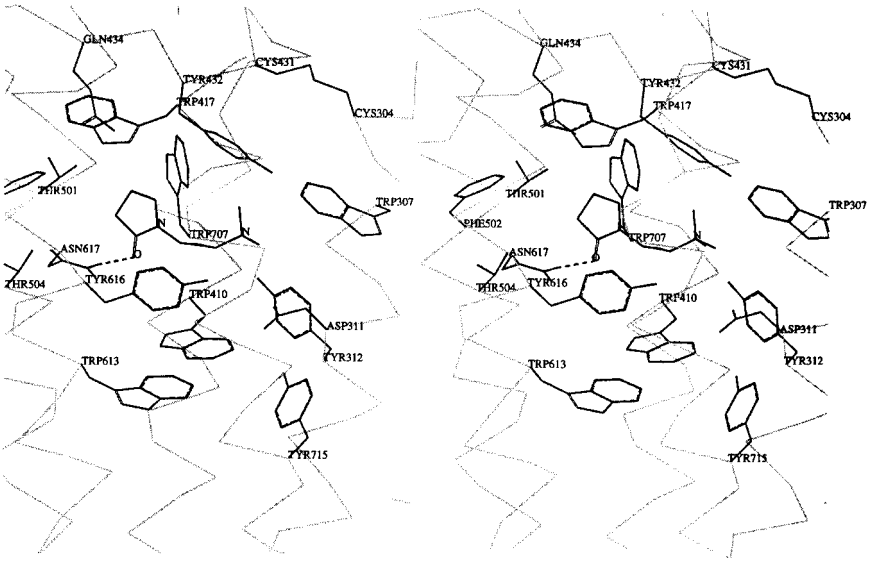

Fig. 6. Stereoplot of oxo-M docked in the binding site of the m_1 muscarinic receptor.

distance between the quaternary ammonium head group and Asp^{311} as compared to oxotremorine, the Trp^{307} side chain is located near the cationic head of the agonist. On the other hand, in addition to the ionic bond with Asp^{311}, the protonated pyrrolidine ring of oxotremorine can form an H-bond with Asp^{311}. Therefore, the pyrrolidine head of oxotremorine is positioned in a subsite different from oxo-M, closer to Asp^{311} and far away from Trp^{307} (Fig. 7).

Docking of the partial agonist McN-A343 was particularly interesting. Although it is much larger than the former agonists, each of its chemical moieties can be accommodated easily, producing complementary interactions with specific residues in the receptor (Fig. 8). The first interaction consists of an H-bond between the carbonyl oxygen of McN-A343 and Asn^{617}. Next, the chloro-substituted phenyl moiety can interact with the extra hydrophobic pocket near the extracellular surface, between helices 3, 4 and 5. This extra hydrophobic pocket is defined by the aromatic residues Phe^{502} located on helix 5, Tyr^{432} on the second extracellular loop and Trp^{417}, which is conserved in at least 85 GPCRs, including the muscarinic receptors. This observation justifies the refinement of the 3D model of the m_1 receptor: in the original model, because of the tilt of helix 4, it was difficult to find a hydrophobic pocket large enough to accommodate the phenyl ring of McN-A343. This pocket, which is not filled in the case of full agonists, may constitute a possible molecular feature that leads to partial agonism.

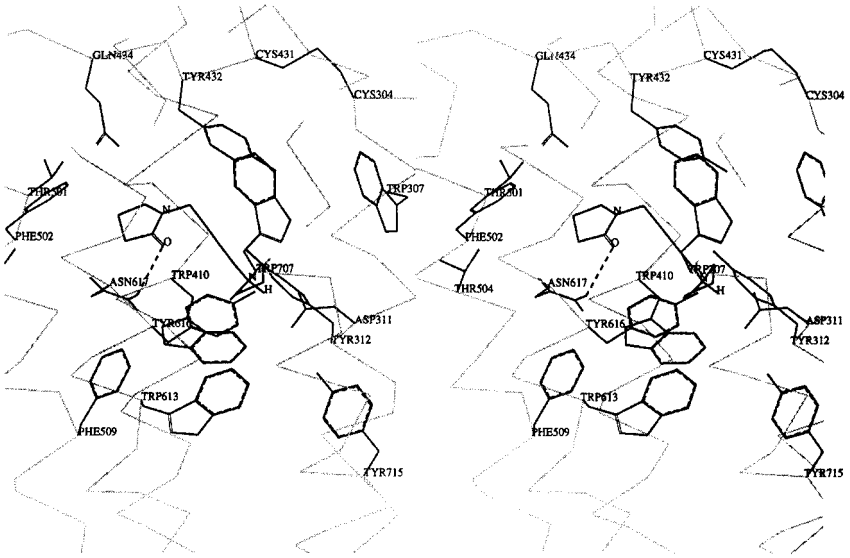

Fig. 7. Stereoplot of oxotremorine docked in the binding site of the m_1 muscarinic receptor.

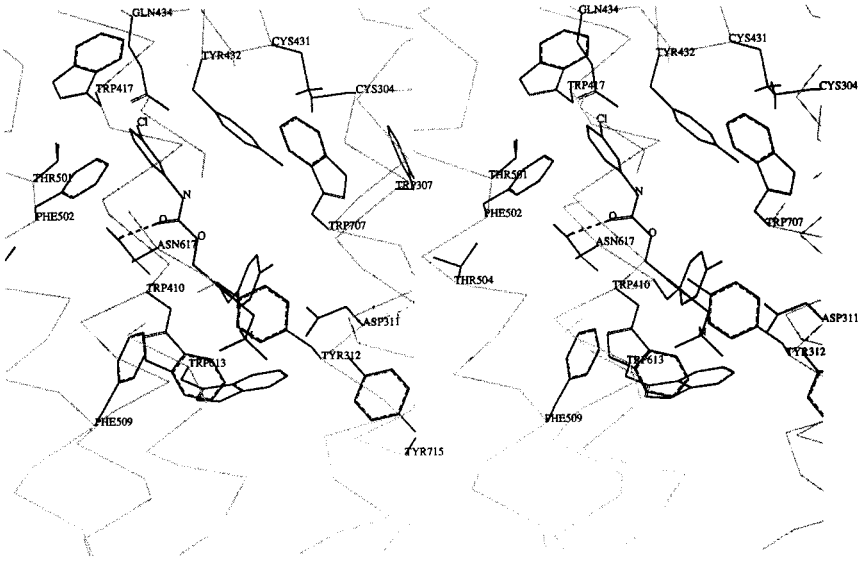

Fig. 8. Stereoplot of McN-A343 docked in the binding site of the m_1 muscarinic receptor.

However, this finding needs to be supported by the study of another series of partial agonists and will be discussed in a subsequent article.

The mutagenesis study led, in some cases, to apparently controversial results. For instance, the Trp^{613}→Phe mutation did not have the same effect on the affinity of the three structurally related agonists oxotremorine, oxo-M and McN-A343: it increased the affinity of oxo-M and McN-A343 but had no influence on the binding of oxotremorine. This suggests that these compounds do not interact directly with Trp^{613}, but preferably in a more indirect manner. Indeed, in the model, the interactions that could have been proposed between these agonists and Trp^{613} do not seem to be possible, due to the very large interaction distance. We can propose that the indirect interactions established by these three agonists with Trp^{613} are highly specific and depend on the physicochemical properties of each ligand. In the case of pilocarpine however, the decrease in affinity obtained by the Trp^{613}→Phe mutation can be directly correlated to a variation of the hydrophobic interactions that can be seen between the methyl group of pilocarpine and Trp^{613} (Fig. 9).

Regarding Asn^{316}, this residue was mutated because it is conserved among the muscarinic receptor family and therefore it could, like Asn^{617}, participate in the binding site by forming an H-bond with one of the common polar areas of the muscarinic ligands. However, the Asn^{316}→Ala

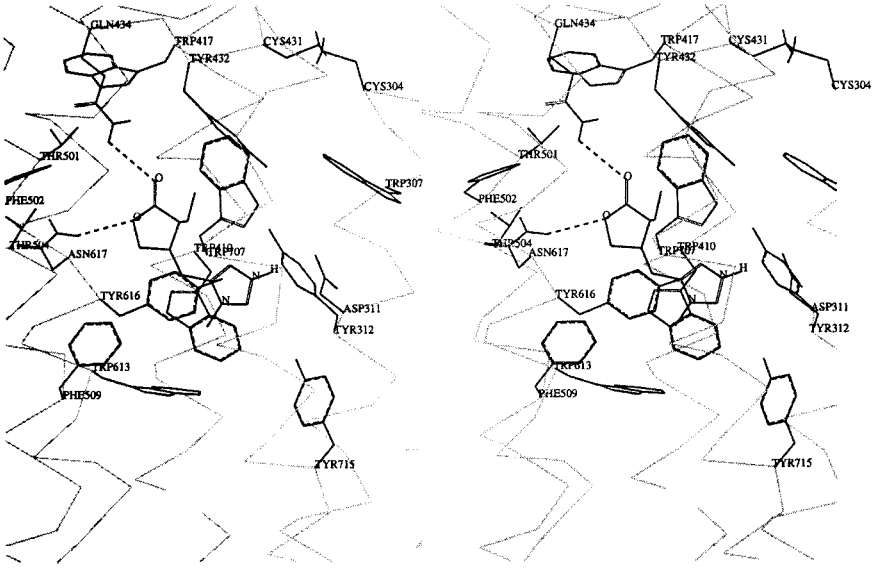

Fig. 9. Stereoplot of pilocarpine docked in the binding site of the m_1 muscarinic receptor.

mutation does not produce the same drastic effect on every tested agonist and antagonist as Asn^{617}→Ala (the most significant change in affinity was a decrease of 31-fold in the affinity of oxo-M). In the 3D model, Asn^{316} can form interhelical H-bonds, thus participating in the overall conformation of the receptor. Thus, its mutation to Ala is likely to lead to a more indirect effect on the binding of ligands. As small agonists do not have the same hindrance in the receptor, they are not affected in the same way by a change in the conformation of the receptor. This might be responsible for the different binding affinities observed in the Asn^{316}→Ala mutant receptor.

Figure 10 shows a superposition of all the tested agonists in their receptor-bound conformation. We can see that although they are concentrated in the same pocket and show similar structures, the different agonists present diverse binding modes. Particularly, there is no exact superposition of the cationic heads and of the two polar areas, in contrast to the muscarinic agonist pharmacophore models proposed by Trummlitz or Hoffmann, where the common electrostatic features can be superimposed [16,34]. We can conclude that the indirect approach used to identify receptor–ligand interactions (i.e. the pharmacophore identification) cannot be considered as a unique mode of investigation. Although the receptor model possesses some specific residues that were experimentally shown to bind the pharmacophoric elements, the different agonists do not bind to the receptor in exactly the same way. Although the conformations extracted from the superimposition are approximately conserved, their orientation in the binding pocket can vary relatively to each other. In fact, the particular structure of each agonist is responsible for its distinct binding mode and for the varying orientation of the side chains of the binding residues that accommodate it.

The antagonists are much larger molecules than the agonists (Fig. 11). They present, in the model, a more similar and rigid binding mode than agonist molecules, which is in agreement with their higher affinity values for the parent receptor (Table 2). Due to their size, the antagonists pirenzepine and 4-DAMP (Figs. 12a and b) fill the whole binding pocket. Indeed, one of their aromatic rings can be located in the hydrophobic pocket at the top of the binding cleft, interacting with residues Phe^{502}, Trp^{417} and Tyr^{432}. The second ring can form strong hydrophobic interactions with Trp^{410} and Tyr^{613} located at the bottom of the binding cleft. This is consistent with the high decrease in affinity obtained by the Trp^{613}→Ala and Trp^{410}→Phe mutations (Table 1). Furthermore, the cationic head of these compounds is located close to Trp^{307}, for which the mutation into Ala decreased the affinity by a factor of 13–29.

Structure–activity relationship studies have shown that in the case of pirenzepine the endocyclic amide function is essential for the interaction with the muscarinic receptor [35]. Indeed, in our model the endocyclic amide group of pirenzepine can form very favorable H-bonds with Asn^{617}. Mutation of this Asn to Ala in the m_1 and m_3 receptors produced mutant receptors which showed a drastically decreased affinity (>100-fold) for pirenzepine. Similarly, in a model of the binding mode of pirenzepine to the human m_1 receptor, an H-bond between the endocyclic function of pirenzepine and Asn^{617} was proposed, on the basis that the Asn^{617}→Asp mutation decreased the affinity of pirenzepine by a factor of 612 [29].

Besides these H-bonds with Asn^{617}, in our model the N4 nitrogen atom of pirenzepine is ideally located to establish an ionic interaction with Asp^{311}. This observation is in agreement with experimental data, which showed that, at physiological pH, pirenzepine is mainly monoprotonated, and this protonation occurs on the N4 nitrogen [35]. Moreover, some analogues of pirenzepine have been synthesized. These molecules only possessed the N4 nitrogen in their structure and were shown to be as active as pirenzepine itself [36].

Like the two other antagonists, NMS has a much larger volume than agonists. Nevertheless, the molecule still has some flexibility and, thus, two possible binding modes can be identified. In the first one (Fig. 12c), the carbonyl oxygen of NMS is involved in an H-bond with Asn^{617}. The phenyl ring of NMS is located at the top of the extra hydrophobic pocket between helices 3, 4 and 5, forming hydrophobic interactions with Phe^{502}, Trp^{417} and Tyr^{432}. In the second binding mode (Fig. 12d), NMS can form two H-bonds with the Asn^{617} residue, with both its carbonyl and hydroxyl functions. The importance of the hydroxyl function in the binding of NMS-like compounds has been demonstrated by Barlow and Ramtoola [37]. In this second possible binding mode, the phenyl ring of NMS forms strong hydrophobic interactions with Trp^{410} and Trp^{613} located at the bottom of the agonist binding site. Actually, mutations of these two residues (Trp^{410}→Phe and Trp^{613}→Ala) lead to a relatively strong decrease in affinity (97- and 115-fold, respectively). In agreement with these findings, the second binding mode seems to be much more plausible.

In both cases, an H-bond could be established between the epoxide moiety of NMS and Tyr^{616} on helix 6. This additional interaction could account for the increase in affinity obtained when the epoxide moiety is added to atropine.

It should be noted that the binding pocket for tricyclic and diphenyl molecules is probably also present in the neurokinin-1 receptor: site-directed mutagenesis studies showed that a histidine residue located on helix 5 of this receptor interacts directly with the benzhydryl of CP-96345, a substance P antagonist, suggesting that other nearby residues within this transmembrane domain should also interact with the antagonist [38].

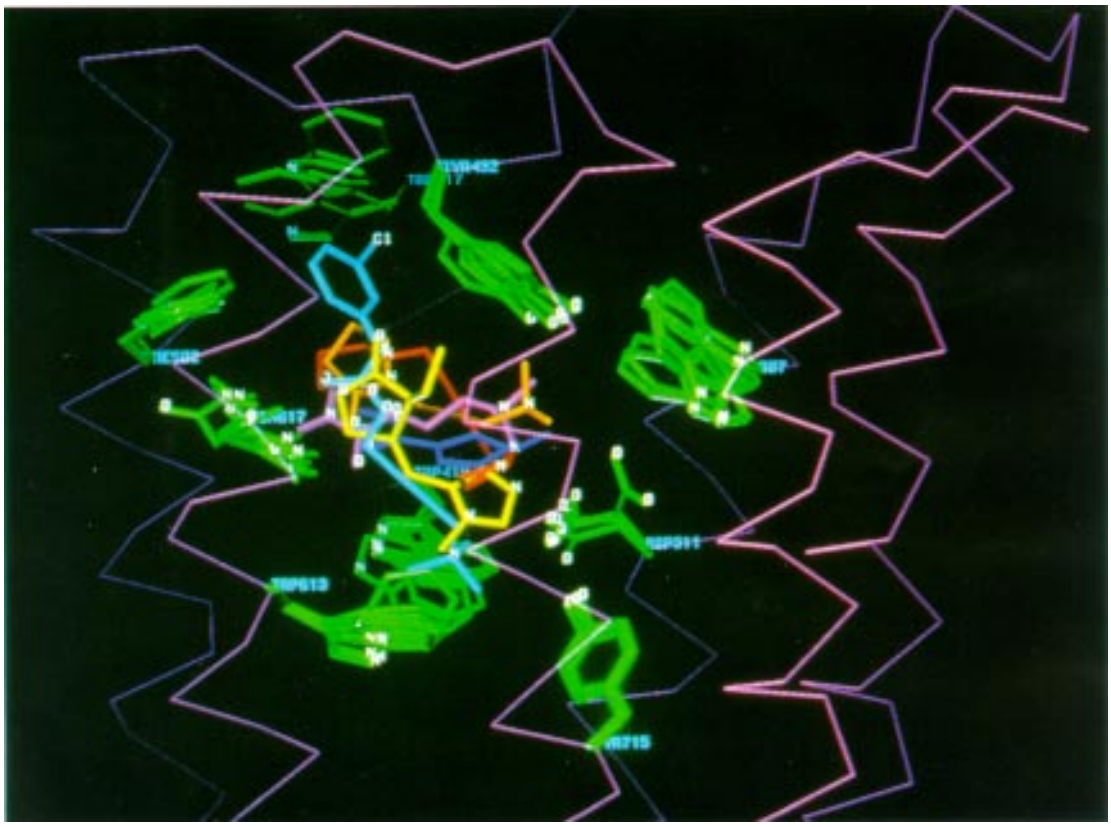

Fig. 10. Superposition view of the complexes made by the tested agonists with the human m_1 receptor model. The color code is as follows: carbachol, pink; oxo-M, orange; pilocarpine, yellow; oxotremorine, red; McN-A343, cyan; arecoline, blue.

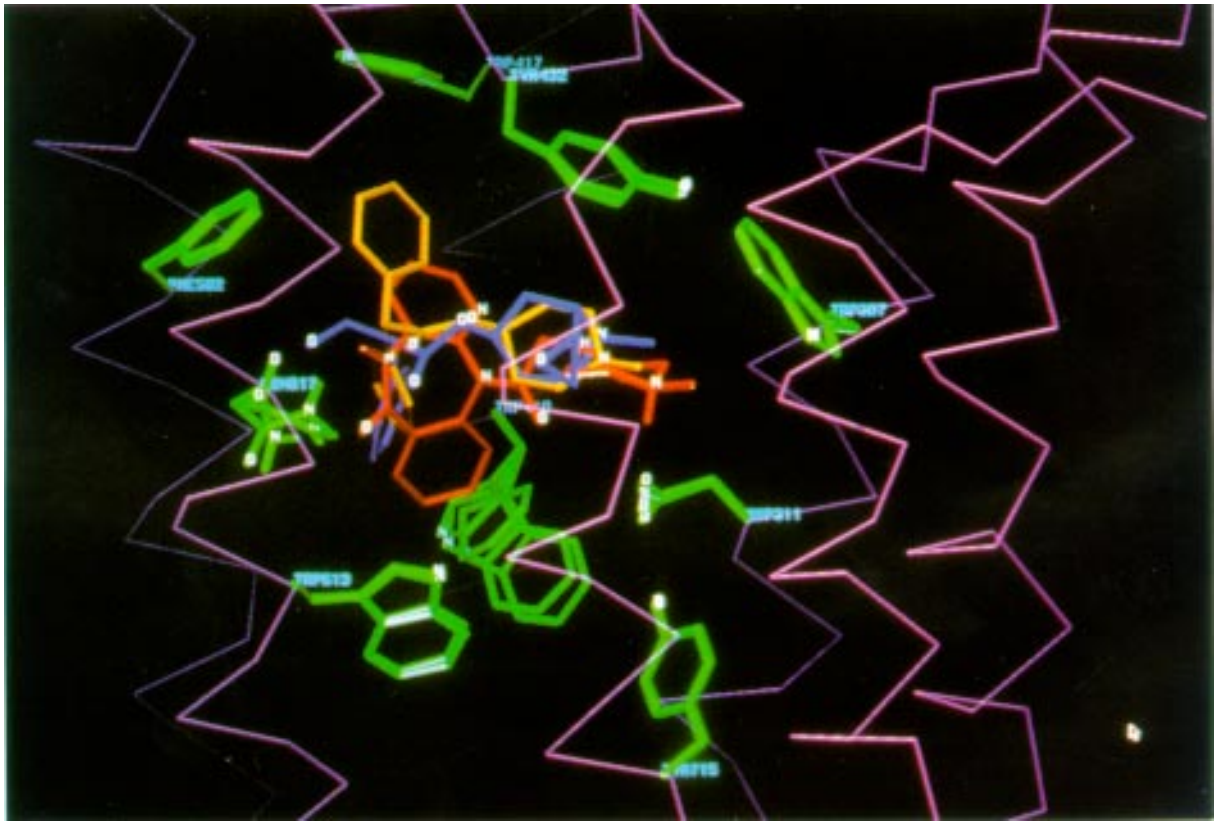

Fig. 11. Superposition view of the complexes made by the tested antagonists with the m_1 receptor. The color code is as follows: pirenzepine, red; 4-DAMP, yellow; NMS, blue.

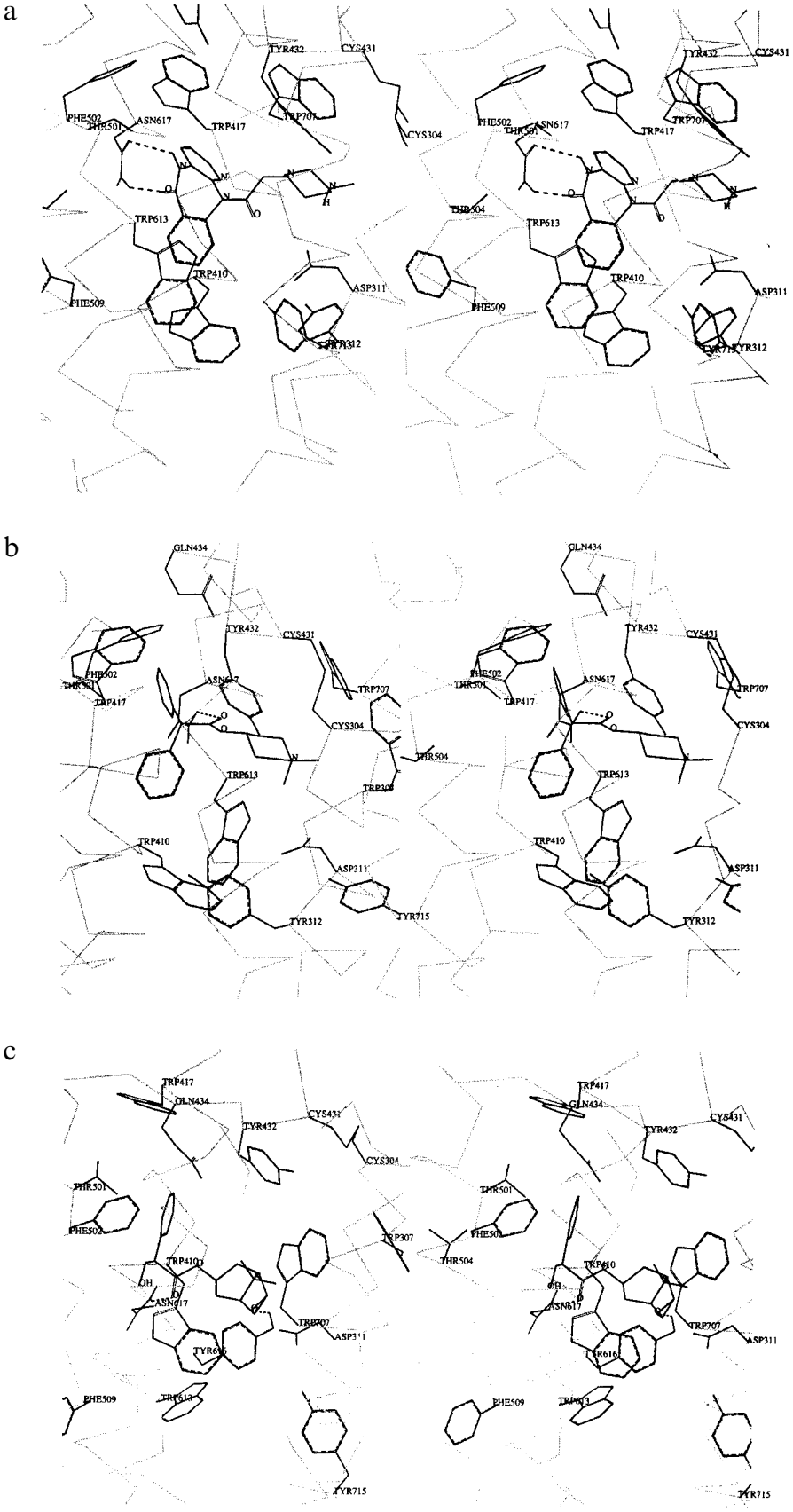

Fig. 12. Stereoplots of the tested antagonists docked in the binding site of the m_1 muscarinic receptor: (a) pirenzepine; (b) 4-DAMP; (c) NMS (first binding mode); (d) NMS (second binding mode).

d

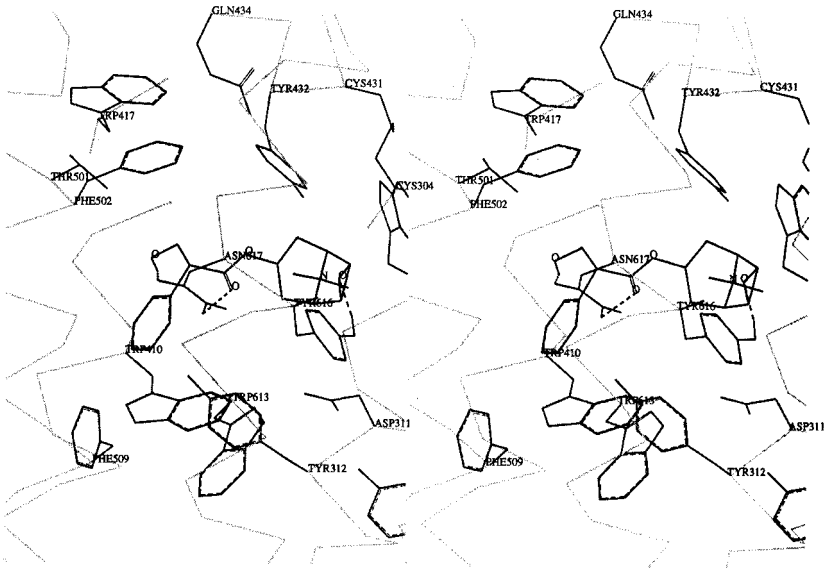

Fig. 12. (continued).

Conclusions

The publication of the first 2D structure of a GPCR, bovine rhodopsin, gave us the opportunity to refine the model we proposed 4 years ago. At the same time, we systematically explored the binding site of the human m_1 muscarinic receptor by site-directed mutagenesis. Combining these two studies, we found that the new optimized model accounts better for these experimental data than the former one. It also shows how subtle receptor–ligand interactions can be.

The mutagenesis studies on muscarinic receptors showed that, in the same receptor subtype, agonists belonging to different structural classes might bind to the same subsite with different local interactions, depending on their structure. More surprisingly, the results, though still controversial, indicate that a given agonist might interact with the same region of different receptor subtypes by using different local anchoring residues: for instance, site-directed mutagenesis studies in the rat m_3 receptor support an H-bond of carbachol with Thr^{504}. On the contrary, in the human m_1 receptor, this threonine does not seem to be involved in the binding of carbachol. On the other hand, the tested tricyclic antagonists seem to bind in the same region as agonists, between helices 3, 4, 5, 6 and 7, and to form the same local interactions in different receptor subtypes.

The refined model and docking assays presented in this study tend to rationalize the experimental data currently available on muscarinic receptor ligands. The agonist binding site is large and allows multiple binding modes for small flexible agonists. The antagonist binding site overlaps those of the agonists, but is additionally composed of a hydrophobic pocket located toward the extracellular part of helices 3, 4 and 5. This pocket can accommodate the phenyl ring of the partial agonist McN-A343 and part of the aromatic region of the diphenyl antagonists pirenzepine and 4-DAMP, the rest of the aromatic region interacting with the bottom of the binding site. Finally, the modelling of the second extracellular loop and especially the disulfide bridge which connects helix 3 to helices 4 and 5 have allowed us to point out some additional residues which seem to participate in the ligand binding site and which can be proposed for new site-directed mutagenesis studies. Overall, there seems to be a good qualitative agreement between simulations and experimental data. However, quantitative prediction of both affinity and efficacy still remains a challenge.

References

1 Nathanson, N.M., Annu. Rev. Neurosci., 10 (1987) 195.
2 Bonner, T., Buckley, N., Young, A. and Brann, M., Science, 237 (1987) 527.
3 Hulme, E.C., Birdsall, N.J.M. and Buckley, N.J., Annu. Rev. Pharmacol. Toxicol., 30 (1990) 633.
4 SYBYL, Tripos Associates Inc., St. Louis, MO, U.S.A., 1994.
5 Trumpp-Kallmeyer, S., Hoflack, J., Bruinvels, A. and Hibert, M., J. Med. Chem., 35 (1992) 3448.
6 Schertler, G.F.K., Villa, C. and Henderson, R., Nature, 362 (1993) 770.
7 Hoflack, J., Trumpp-Kallmeyer, S. and Hibert, M., Trends Pharmacol. Sci., 15 (1994) 7.
8 Baldwin, J., EMBO J., 12 (1993) 1693.
9 Brunger, A.T., X-PLOR Manual, v. 3.0, Yale University, New Haven, CT, U.S.A., 1992.
10 Jones, T.A., Methods Enzymol., 115 (1985) 57.
11 Weiner, S.J., Kollman, P.A., Case, D.A., Singh, U.C., Ghio, C., Alagona, G., Profeta Jr., S. and Weiner, P., J. Am. Chem. Soc., 106 (1984) 765.
12 Cambridge Crystallographic Data Centre, Cambridge CB2 1EZ, U.K.

13 Allen, F.H., Kennard, O. and Taylor, R., Acc. Chem. Res., 16 (1983) 146.
14 Melchiorre, C., Minarini, A., Budriesi, R., Chiarini, A., Spampinato, S. and Tumiatti, V., Life Sci., 11/12 (1995) 837.
15 Dewar, M.J.S., Zoebish, E.G., Healy, E.F. and Stewart, J.J.P., J. Am. Chem. Soc., 107 (1985) 3902.
16 Hoffmann, R., Bourguignon, J.J. and Wermuth, C.G., Pharmacochem. Libr., 16 (1991) 283.
17 Showell, G.A., Tracey, L.G., Kneen, C.O., MacLeod, A.M., Merchant, K.J., Saunders, J., Freedman, S.B., Patel, S. and Baker, R., J. Med. Chem., 34 (1991) 1086.
18 Hibert, M., Trumpp-Kallmeyer, S., Bruinvels, A. and Hoflack, J., Mol. Pharmacol., 40 (1991) 8.
19 Henderson, R., Baldwin, J.M. and Ceska, T.A., J. Mol. Biol., 213 (1990) 899.
20 Grigorieff, N., Ceska, T.A., Downing, K.H., Baldwin, J.M. and Henderson, R., J. Mol. Biol., 259 (1996) 393.
21 Kenakin, T., Trends Pharmacol. Sci., 16 (1995) 188.
22 Curtis, C.A.M., Wheatley, M., Bansal, S., Birdsall, N.J.M., Eveleigh, P., Pedder, E.K., Poyner, D. and Hulme, E.C., J. Biol. Chem., 264 (1989) 489.
23 Matsui, H., Lazareno, S. and Birdsall, N.J.M., Mol. Pharmacol., 47 (1995) 88.
24 P9 poster, 7th Swiss Workshop of Methodology in Receptor Research, 1996.
25 Olah, M.E., Jacobson, K.A. and Stiles, G.L., J. Mol. Biol., 269 (1994) 24692.
26 Hulme, E.C., Curtis, C.A.M., Page, K.M. and Jones, P.G., Life Sci., 11/12 (1995) 891.
27 Wess, J., Gdula, D. and Brann, M.R., EMBO J., 10 (1991) 3729.
28 Wess, J., Nanavati, S., Vogel, Z. and Maggio, R., EMBO J., 12 (1993) 331.
29 Murgolo, N.J., Kozlowski, J., Tice, M.A.B., Hollinger, F.P., Brown, J.E., Zhou, G., Taylor, L.A. and McQuade, R.D., Bioorg. Med. Chem. Lett., 6 (1996) 785.
30 Dixon, R.A.F., Strader, C.D. and Sigal, I.S., Annu. Rep. Med. Chem., 23 (1988) 221.
31 Bluml, K., Mutschler, E. and Wess, J., J. Biol. Chem., 29 (1994) 18870.
32 Nordvall, G. and Hacksell, U., J. Med. Chem., 36 (1993) 967.
33 Fanelli, F., Menziani, M.C., Carotti, A. and De Benedetti, P.G., Bioorg. Med. Chem., 3 (1994) 195.
34 Kier, L.B., Mol. Pharmacol., 3 (1967) 487.
35 Eberlein, W.G., Trummlitz, G., Engel, W.W., Schmidt, G., Pelzer, H. and Mayer, N., J. Med. Chem., 30 (1987) 1378.
36 Quintero, M.G., Donetti, A., Giachetti, A., Ladinsky, H., Limonta, P., Micheletti, R. and Schiavi, G.B., IXth International Symposium on Medicinal Chemistry, West Berlin, Abstract Book, 1986.
37 Barlow, R.B. and Ramtoola, S., Br. J. Pharmacol., 71 (1980) 31.
38 Fong, T.M., Cascieri, M.A., Yu, H., Bansal, A., Swain, C. and Strader, C.D., Nature, 362 (1993) 350.